We are IntechOpen, the world's leading publisher of Open Access books
Built by scientists, for scientists

6,900
Open access books available

186,000
International authors and editors

200M
Downloads

154
Countries delivered to

Our authors are among the

TOP 1%
most cited scientists

12.2%
Contributors from top 500 universities

CLARIVATE ANALYTICS
BOOK CITATION INDEX
INDEXED

WEB OF SCIENCE™

Selection of our books indexed in the Book Citation Index
in Web of Science™ Core Collection (BKCI)

Interested in publishing with us?
Contact book.department@intechopen.com

Computer-Aided Design of Microwave-Photonics-Based RF Circuits and Systems

Mikhail E. Belkin, Vladislav Golovin, Yuri Tyschuk,
Mikhail G. Vasil'ev and Alexander S. Sigov

Additional information is available at the end of the chapter

Abstract

In the process of design, a developer of new microwave-photonics-based RF apparatuses is facing a problem of choosing appropriate software. As of today, the existing optical and optoelectronic CAD tools (OE-CAD) are not developed like CAD tools intended for modeling of RF circuits (E-CAD). On the contrary, operating at symbolic level, modern high-power microwave E-CAD tools simply and with high precision solve this problem, but there are no models of active photonic components in their libraries. To overcome this problem, we proposed and validated experimentally a new approach to model a broad class of promising analog microwave radio-electronics systems based on microwave photonics technology. This chapter reviews our known, updated, new models and simulation results using microwave-electronics off-the-shelf computer tool NI AWRDE to pursue advanced performances corresponding to the last generation of key photonics structural elements and important RF devices on their basis.

Keywords: computer-aided design, microwave photonics, photonic components, RF circuits and system

1. Introduction

Microwave photonics (MWP) is a relatively fresh scientific and technological direction arising among radio-electronic R&D society at the last quarter of twentieth century in the result of combining the achievements of microwave-electronics and photonics techniques [1]. Initially, MWP was an area of interest for a military platform [2, 3] such as radar and electronic warfare means; but, nowadays, it is becoming an object of study and development for emerging areas of telecom industry [4] such as 5G-class wireless networks. For today, MWP technology might

be considered as a perspective direction of modern radio-electronics for signals generation, transmission, and processing in various radio-frequency (RF) circuits and systems. Implementation of this concept will enhance the key technical and economical features and such important characteristics as electromagnetic and environmental compatibilities, immunity to external interferences.

Figure 1 demonstrates a typical MWP circuit that is started with RF-to-optical converter (RF/O) and concluded with optical-to-RF converter (O/RF). Between these interfaces, there are a host of efficient photonics processing units in optical domain.

In the process of design, a developer of new MWP-based RF apparatuses is facing a problem of choosing an appropriate software. As of today, the existing optical and optoelectronic CAD tools (OE-CAD) are not developed like being perfected for three decades CAD tools intended for modeling of RF circuits (E-CAD). On the contrary, operating at symbolic level modern high-power microwave E-CAD tool solves this problem enough simply and with high precision, but there are no models of specific active and passive photonic components in its library. To overcome this problem, we have been proposed and validated experimentally a new approach to model a broad class of promising analog microwave radio-electronics systems based on the microwave photonics technology. In particular, the classification of active photonic components and the comparison with a modern OE-CAD tool were described in Ref. [5] and later in more detail version in Ref. [6]. Based on them, the electrical equivalent circuit models for the different types of semiconductor laser [7, 8], photodetector [9, 10], and optical modulator of Mach-Zehnder interferometer configuration [6] were published. Using these components, a number of RF circuit models and successful simulation results for microwave-band optoelectronic oscillator [11], mixer [12], and phased array antenna beam-former network [13] were proposed.

The general concept behind the design is the following. A developer of these novel RF circuits has no basic knowledge about the physical features of active and passive photonic devices, but one has a toolset to measure carefully their transmission characteristics in linear and nonlinear modes. Based on it, the design principles of the equivalent-circuit models to be considered below fully reflect the common building principle of the available E-CAD tools including closed-form or table-specified library models of current and voltage sources, nonlinear active devices, as well as passive elements that subject to frequency band are built on a linear circuitry with lumped (for RF band) or distributed (for microwave and millimeter-wave bands) parameters.
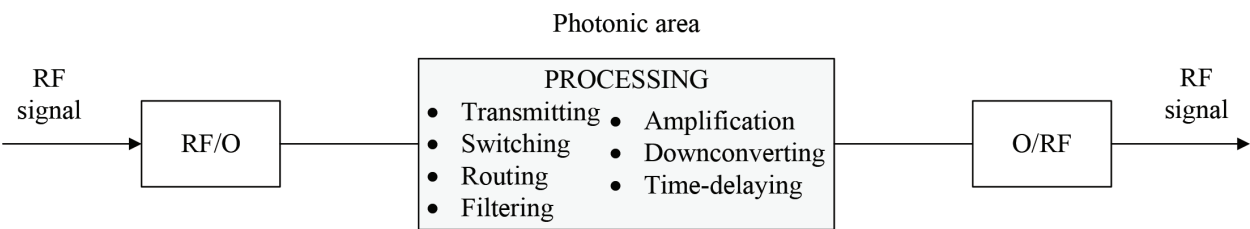

Figure 1. A typical arrangement of MWP circuit.

This chapter reviews our updated and new equivalent-circuit-based models and simulation results using microwave-electronics off-the-shelf computer tool NI AWRDE to pursue advanced performances corresponding to the last generation of key MWP photonics structural elements and important devices on their basis. In particular, Section 2 describes two laser models referred to direct RF-to-optical conversion. In addition, Section 3 presents three optical modulator models for the case of external RF-to-optical conversion. There is a description of two models for optical-to-RF conversion realized by the equivalent-circuit models of photodetector component in Section 4. The component part concludes the discussion of the specific models for optical passives in Section 5. Following the result of the previous sections, some advanced MWP-based RF circuits are modeled in Section 6. Finally, Section 7 concludes the chapter.

2. Direct RF-to-optical conversion

As well known, in a digital fiber-optic communication link, injection-current driven semiconductor laser is a requisite for simple direct conversion to optical band with the speeds up to 10 Gbit/s. In this case, a laser operates in bi-stable mode with two transmitting positions: optical emission is switched off when the injection current is below the threshold of the laser light-current plot (LCP) or is switched on when it is beyond the threshold of the LCP. The main distinguish feature of MWP link, which is a medium for analog RF-signal transmission, is in continuous mode operation presetting DC bias in the middle of LCP's linear area that provides a different approach to design. Below, we demonstrate two laser models usable for various microwave photonic circuits.

2.1. Single-carrier laser model

Figure 2 depicts updated nonlinear model of a semiconductor laser emitter in the form of an electric equivalent circuit, suitable for developers of RF-subcarriers modulated analog fiber-optics systems, devices of microwave optoelectronics, as well as optical interconnects in the
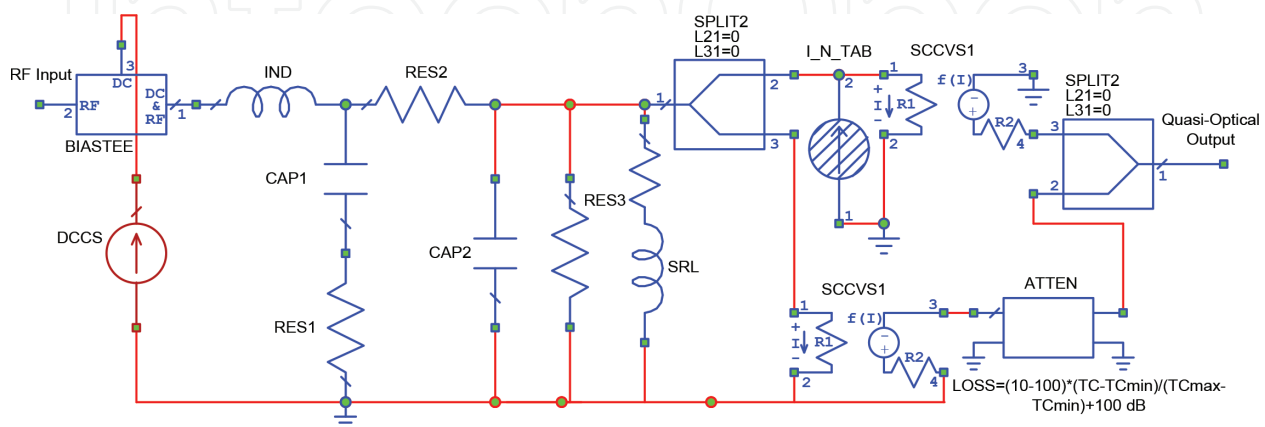

Figure 2. Single-carrier model of a semiconductor laser in the form of an equivalent circuit.

integrated circuits. In this circuit model, each element has a clear physical interpretation. Namely, the active circuitry in according to the previous versions [7, 8] includes library models of DC current source DCCS to adjust operation point, polynomial-approximated SPICE current-controlled voltage source SCCVS1 imitating laser's LCP, and the noise source I_N_TAB allowing to take into account the noise properties of the laser, which are usually expressed in the form of relative intensity noise (RIN) or relative phase noise. Data for the source are specified in tabular form from the results of measurements. Besides, RF input through ideal model of bias-T element (BIASTEE) connects to inductor model (IND) emulating a wire from RF-connector to laser chip. The laser chip itself is represented by elements CAP1 and RES1 simulating the pad capacitance and loss, series resistance RES2, junction capacitance and resistance, and CAP2 and RES3, respectively, and element SRL represents the laser mirror losses and photon storage effects. Notice that the values of all abovementioned passive elements simulate frequency response of RF-to-optical conversion. As a new function, the dependence of the output power on the ambient temperature is added, which makes the model under simulation more suitable for real systems. The temperature drift of the LCP in the circuit is realized on the basis of two models of ideal splitters SPLIT2, the lower unit of SCCVS1, which output is in antiphase relative to the main channel, and the model of attenuator ATTEN, the value of which is a function of a temperature.

Using the proposed model together with a reference photodetector, a set of typical for radio-engineering circuit simulation experiments is able to fulfill including signal transmitting characteristics (S_{21} and S_{11}), noise figure, nonlinearity due to harmonic or intermodulation distortions, and so on. **Figure 3** exemplifies the simulation results of small-signal frequency response (a) and LCPs in the temperature range of 20–70°C (b).

2.2. Multi-carrier laser model

As noted, the great advantage of photonic technology in comparison with the radio-electronic counterpart is the ultra-wide bandwidth of optical fiber, exceeding 10 THz. Following it, in modern MWP circuits, the so-called method of wavelength division multiplexing (WDM) is
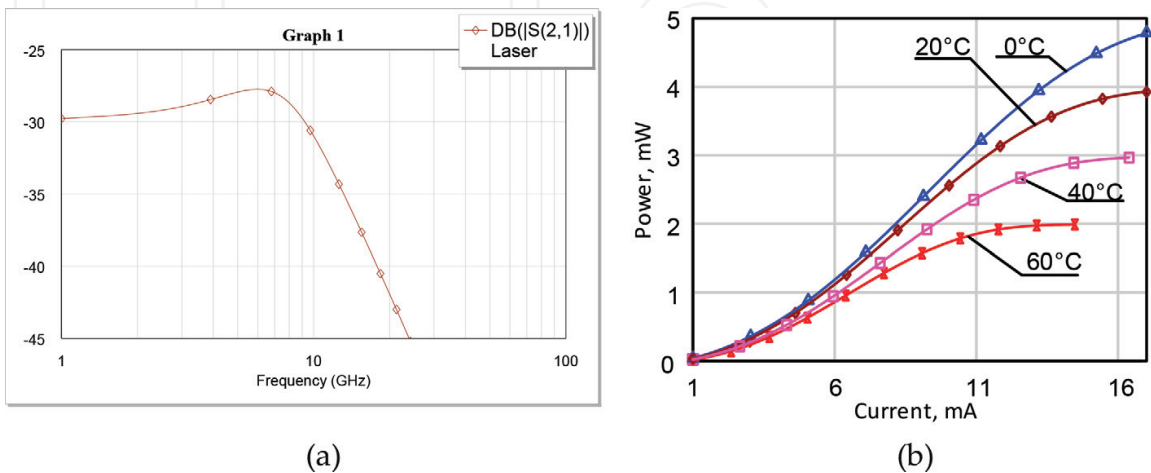

(a)   (b)

Figure 3. The examples of simulation experiments: (a) small-signal frequency response, and (b) light-current plot.

widely used [14], in which simultaneous transmission of information on a plurality of optical carriers is provided. The lack in aptitude does not allow the previous model to design correctly multi-carrier MWP circuits and has led to a new generation of laser model feasible for WDM circuit simulation [5, 6]. **Figure 4** depicts the updated nonlinear model of a semiconductor laser emitter suitable for MWP WDM circuits and systems. The model has the simplest configuration including only one quasi-optical (QO) unmodulated carrier and one RF signal but its building principle allows aggregating both optical and RF channels.

In contrast to the model of **Figure 2**, this model has two main input ports titled as "Quasi-Optical Input 1" and "RF Input"; the first one receives waveforms of optical band and the second one is for waveforms of RF-band. Such an approach is correct for a software tool working at the symbolic level. The chain of RF channel consists of sub-circuit network (SUBCKT) including the schematic of **Figure 2** and the model of 9-order Butterworth bandpass filter (BPFB1), which is designed to eliminate spurious output signals of the subcircuit. In line with the standard radio engineering approach, both signals are then mixed using an ideal full-wave diode multiplier. Another model of the BPFB2 with modulated QO signal at the Quasi-Optical Output is terminated by the circuit. In the model, the dependence of the QO carrier frequency versus temperature is additionally introduced, which is realized by means of an additional Quasi-Optical Input 2. The main (foptic-1000 GHz, port 1) and the additional
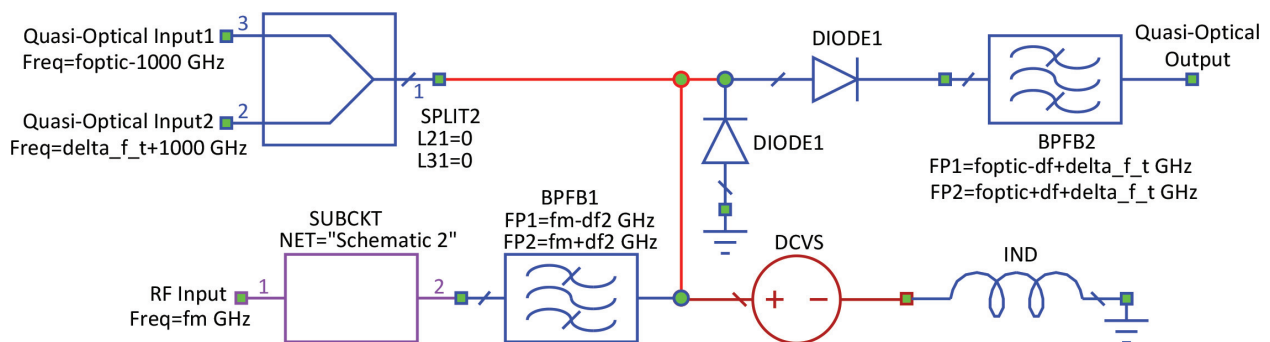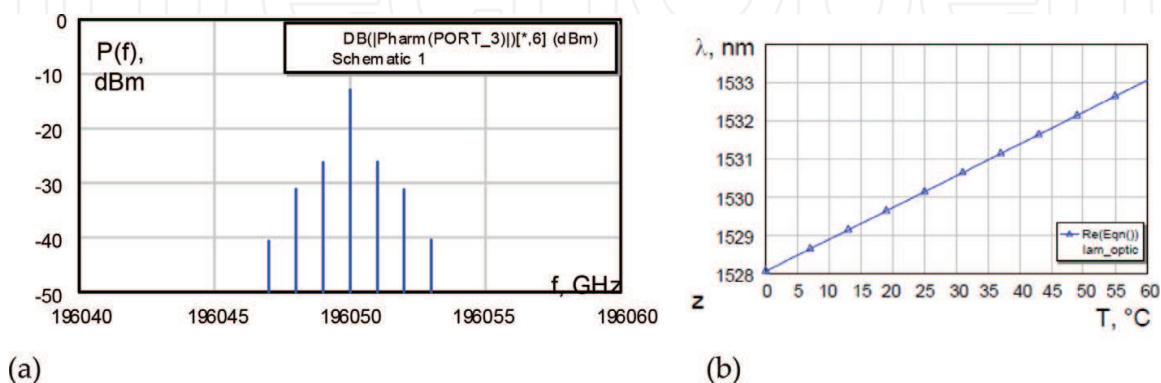

Figure 4. Double-carrier laser model.

Figure 5. The examples of simulation experiments.

(delta_f_t + 1000 GHz, port 2) signals are fed to the diode multiplier. The value of the auxiliary frequency depends on the factor delta_f_t, which describes the experimental emitted wavelength-temperature dependence of the laser chip. The frequency band of the FPFB2 is also corrected taking into account this factor. **Figure 5** exemplifies the simulation results of output laser spectrum modulated by RF tone of 1 GHz and power 10 dBm (a) and wavelength versus temperature dependence in the range of 0–60°C (b).

3. External RF-to-optical conversion

In spite of cost-efficiency, the direct RF-to-optical conversion has a number of limiting factors including bandwidth, dynamic range, chirping (parasitic frequency modulation), etc. To overcome them, as in radio engineering technique, an external RF-to-optical conversion using a separate device titled "optical modulator" is in common practice for MWP circuits. As in RF systems, there are two classes of optical modulators: phase and amplitude ones; the latter in connection with the specialties of lightwave transmission called "the intensity modulator". Building principles and layouts of microwave-band optical modulators as well as initial equivalent-circuit models are described elsewhere [6]. Below, two updated models of optical phase modulator (OPM) and Mach-Zehnder interferometer-based optical intensity modulator (MZM), as such as a novel model for so-called electro-absorption intensity modulator (EAM), are demonstrated and discussed.

3.1. Optical phase modulator model

The core element of OPM model is the phase-shifting cell (PSC). **Figure 6** depicts the equivalent circuit of PSC, where the phase shift is simulated by the library varactor model VRCTR, whose nonlinear characteristic is extracted from the measured data. The phase shift of the quasi-optical signal is fed to the cell output via a diplexer acting as a high-pass filter. The
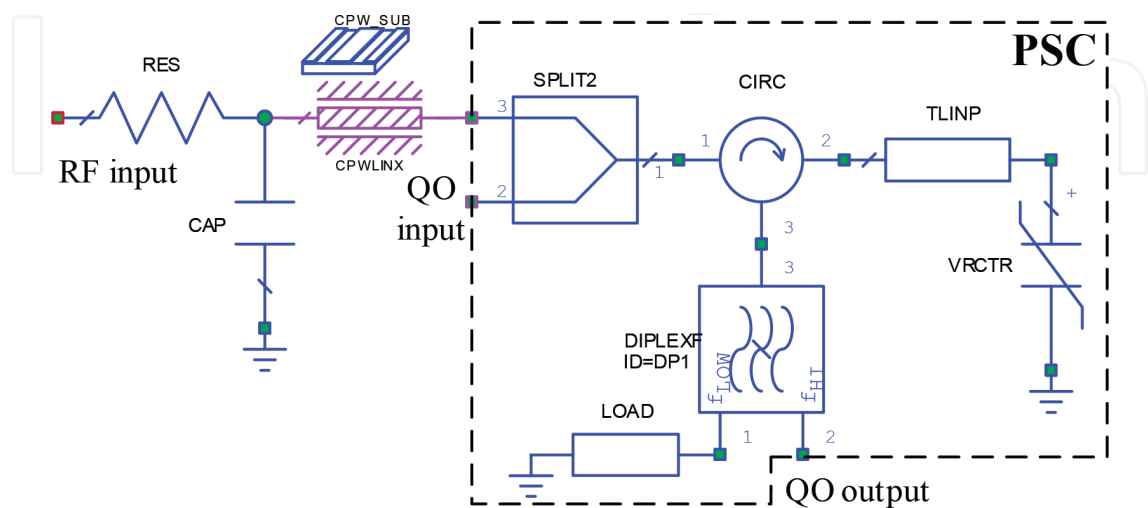

Figure 6. The model of phase-shifting cell.

difference from the known model [6] is the larger correctness due to the introduction of library models of transmission line with frequency-dependent loss TLINP, symmetric coplanar line with table-based interpolation CPWLINX, and so on.

Figure 7 shows the equivalent model of optical phase modulator including PSCs as subcircuits. The number of PSCs is increased to 4 to provide a quasi-linear adjustment of the insertion phase shift within more than 180°, typically required for OPM operation. The resulting phase shift is formed in the OPM as the algebraic sum of the phase shifts of the each PSC, since the signal at the optical frequency sequentially passes through all the cells.

Figure 8 exemplifies the simulation results demonstrating the linearity of the phase shift versus control voltage in PSC (a) and 35-dB suppression of higher harmonics in output spectrum (b).
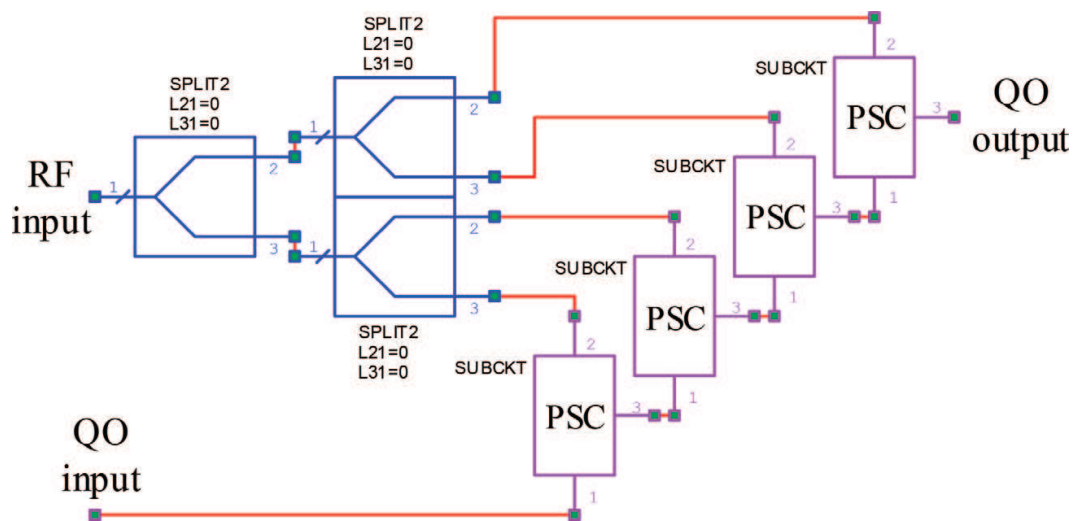

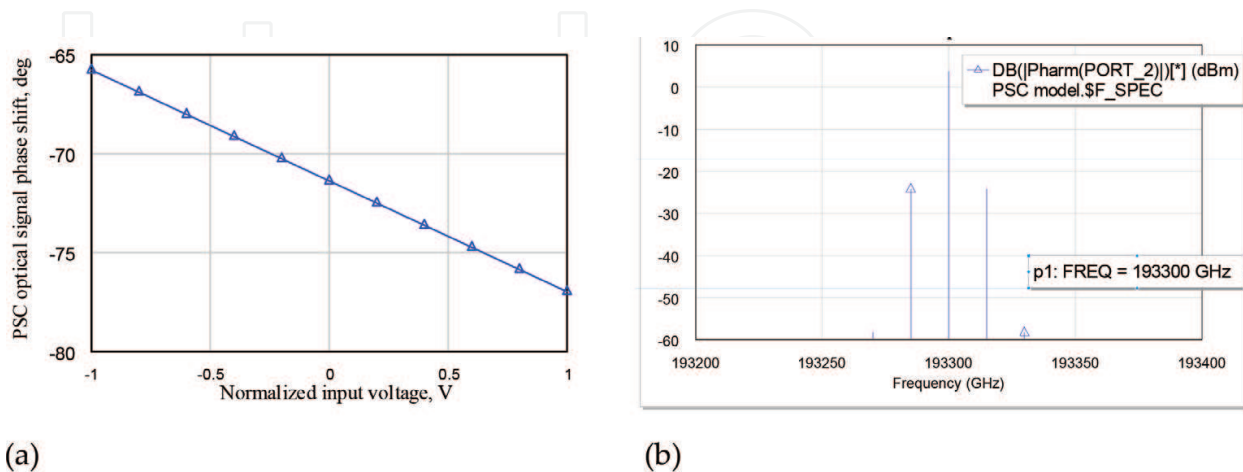**Figure 7.** Model of optical phase modulator.

(a)   (b)

Figure 8. The examples of simulation experiments: (a) phase-voltage dependence of PSC and (b) quasi-optical spectrum at OPM output.

3.2. Mach-Zehnder interferometer-based intensity modulator model

As is known [6], an optical intensity modulator of a MZM type contains a two-arm interferometer, in each arm of which an optical phase modulator is introduced. **Figure 9** depicts the AWRDE model of optical MZM with two OPMs of **Figure 7** as subcircuits. Inside it, the RF signal is applied in antiphase to the inputs of both OPMs via the coplanar transmission line CPWLINX and the ideal splitter SPLIT2. The output channel of one of the OPMs includes two phase-shifter library elements PHASE2, of which the first is responsible for setting the operating point on the MZM transfer characteristic and the second PHASE2 adjusts a fixed phase difference in the arms of realistic MZM. The interference of two phase-modulated signals is carried out at the output of the splitter model SPLIT2. The output attenuator is used to calibrate the power loss of the optical signal introduced by the MZM.

Figure 10 exemplifies the simulation results demonstrating the advantage in the bandwidth and linearity of the external RF-to-optical conversion using a MZM compared to direct one. In particular, **Figure 10(a)** simulates the optical modulated spectrum using the RF tone of 15 GHz and the same input power as in Section 2.2. Comparison with **Figure 5(a)** shows an increase in
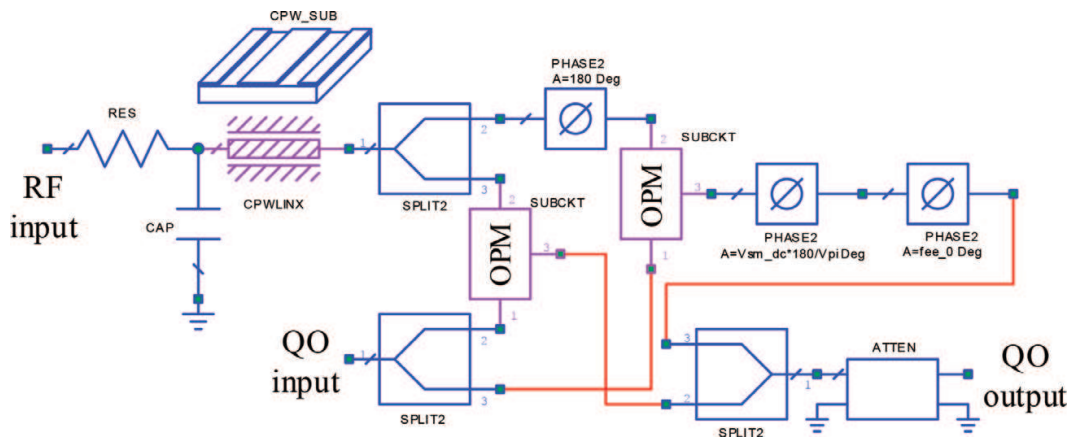

Figure 9. Mach-Zehnder interferometer-based intensity optical modulator model.
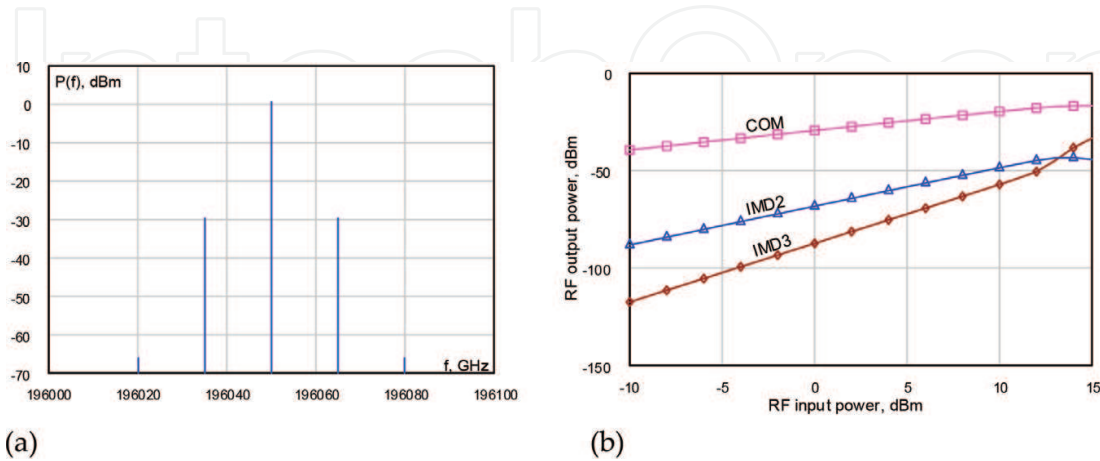

Figure 10. The examples of simulation experiments: (a) optical modulated spectrum and (b) large-signal transmission characteristics.

the suppression of the second harmonic by more than 30 dB. Besides, **Figure 10(b)** simulates the dependence of RF output power (after ideal optical-to-RF conversion) on input RF power for the fundamental RF modulation tone (COM), 2-order intermodulation distortion (IMD2), and 3-order intermodulation distortion (IMD3) that shows the better linearity feature than a power microwave transistor.

3.3. Electro-absorption effect-based intensity modulator model

In spite of high linearity of RF-to-optical conversion, the main shortcoming of MZM is bulky sizes, which is a concern for a number of very important radio engineering applications. An intriguing solution to the problem is the usage of an electro-absorption intensity modulator (EAM) that can be integrated with a laser chip [15]. **Figure 11** depicts the AWRDE model of optical EAM. The nonlinear model of EAM is implemented based on the modified Materka field effect transistor (MATRK) library model. The EAM model includes two MATRK elements, which are controlled by a RF signal and act as attenuators that are connected in serious to the quasi-optical channel. The use of two MATRK elements provides deep intensity (amplitude) modulation of the optical carrier. The limits of the dynamic range for the input signals are determined by the selection of the parameters of the library resistor models (RES). The circuit is terminated by BPFB and closed-form amplifier (AMP) library models to eliminate higher harmonics and calibrate the loss inserted by the EAM path (for AMP, any gain value including less than 0 dB could be set). In addition, there are three ideal isolator models (ISOL8R) to ensure the isolation of the inputs and outputs.

Figure 12 exemplifies the simulation results demonstrating the advantage in the bandwidth and linearity of the external RF-to-optical conversion using an EAM compared to direct RF/O one but some disadvantage in compare to external RF/O conversion by a MZM. In particular, **Figure 12(a)** simulates the optical modulated spectrum using the RF tone of 10 GHz and the same input power as in Section 2.2. Comparison with **Figure 5(a)** shows an increase in the suppression of the second harmonic by more than 20 dB. Besides, **Figure 12(b)** simulates the dependence of RF output power (after ideal optical-to-RF conversion) on input RF power for the fundamental RF modulation tone (COM), 2-order intermodulation distortion (IMD2), and 3-order intermodulation distortion (IMD3) that shows the linearity features compared to middle power microwave transistor.
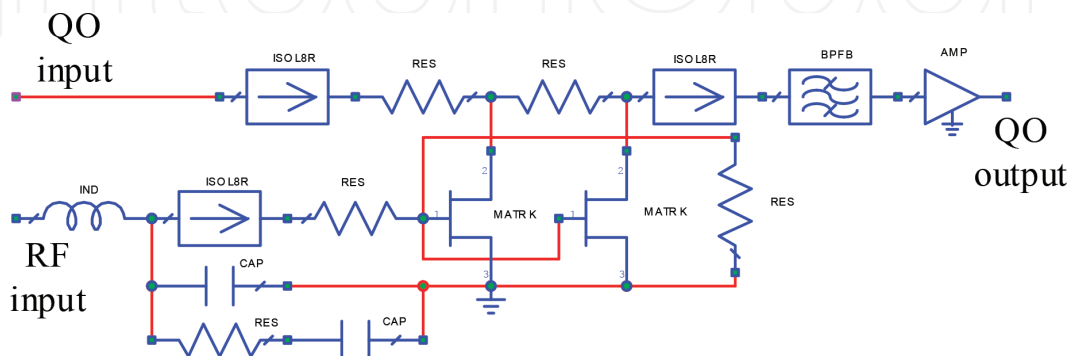

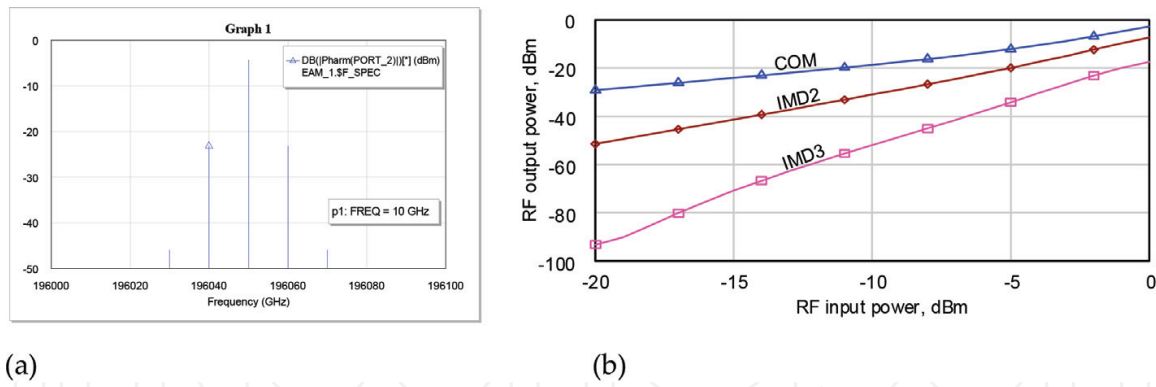**Figure 11.** Electro-absorption effect-based intensity modulator model.

Figure 12. The examples of simulation experiments: (a) optical modulated spectrum and (b) large-signal transmission characteristics.

4. Direct optical-to-RF conversion

Nowadays, there is a plurality of direct optical-to-RF conversion elements (photodetectors) but only photodiodes of so-called PIN structure are in common use for analog fiber-optic systems. Among them, long wavelength GaInAs-based PIN photodetectors (PD) are ubiquitous in modern MWP circuits due to their inherent combination of ultra-high speed, high sensitivity, and linearity features [16]. Early, we described and studied in detail the AWRDE nonlinear model of microwave-band PIN PD [9, 10]. **Figure 13** shows the updated more realistic PD model where noise sources (INOISE) including shot noise of photodiode and heat noise of the equivalent resistors (RES) are taken into account. From the viewpoint of the RF circuitry, a PIN PD can be modeled as a current source with high output impedance that is imitated by the library model of voltage controlled current source (VCCS). Besides, the nonlinear features are emulated by temperature-dependent diode model (DIODE1) and barrier capacitance of p-n junction (PNCAP) tunable in according with applied reverse voltage from DCVS model. The linear circuitry representing the frequency distortions due to stray PD elements agrees with small-signal PD model that was described elsewhere [17].
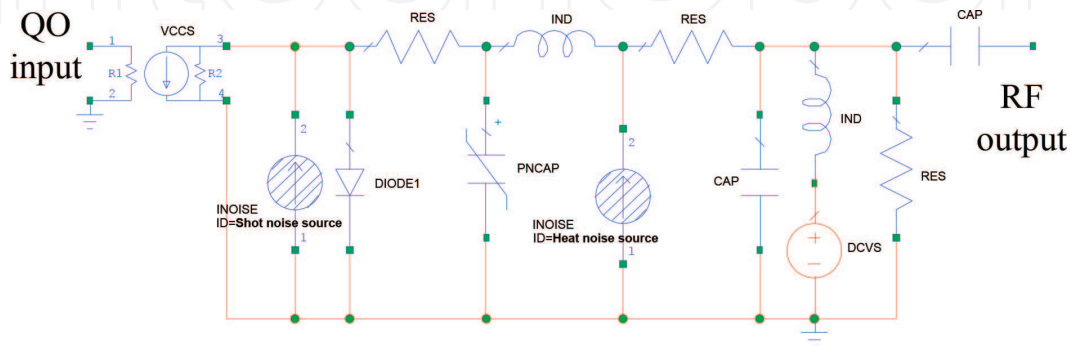

Figure 13. AWRDE nonlinear model of microwave-band PIN photodetector.

The collection of photo-detecting elements includes a number of advanced constructions. The most feasible among them is a balanced one that has an advantage of more linear O/RF conversion [14]. **Figure 14** depicts the AWRDE model of a balanced photodetector.

As well-known from radio-engineering technique, the circuit consists of two arms and each of them includes the photodetector model of **Figure 13** as subcircuit. To provide antiphase excitation of the subcircuits, there is a library reciprocal model of phase shifter PHASE2 in the upper arm. **Figure 15** exemplifies the simulation results for the both types of direct O/RF conversion elements under consideration. In particular, **Figure 15(a)** simulates small-signal frequency response ($|S_{21}|$) of realistic PD using **Figure 13**'s model. As seen, the 3-dB bandwidth is near 20 GHz. Besides, **Figure 15(b)** simulates the dependence of RF output power on input RF power (before ideal RF-to-optical conversion) for the fundamental RF modulation tone (COM) and 3-order intermodulation distortions for the models of **Figure 13** (line 1) and **Figure 14** (line 2). In the figure, one can see two characteristic cross-points of the lines 1 and 2 with the line "COM." These points are termed as output intercept points of 3-order (OIP3) representing very important metric of O/RF conversion linearity [14]. Following the results, one can conclude that firstly, photodetector demonstrates the most linear conversion feature in compare to MZM (**Figure 10(b)**) or EAM (**Figure 12(b)**) and secondly, balanced version of
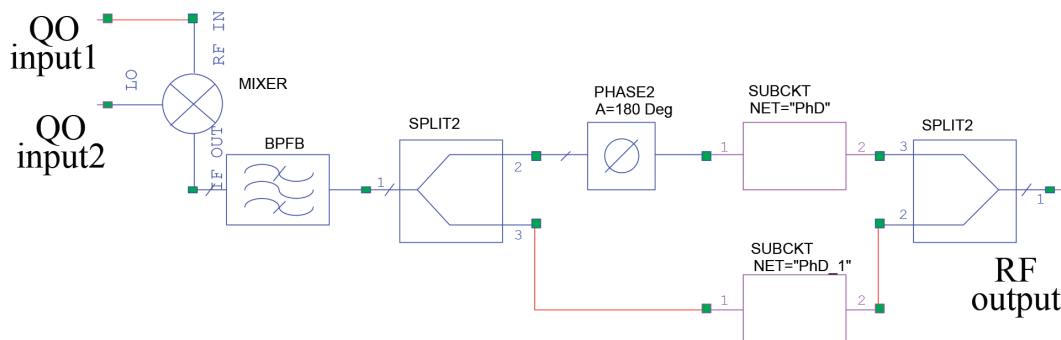

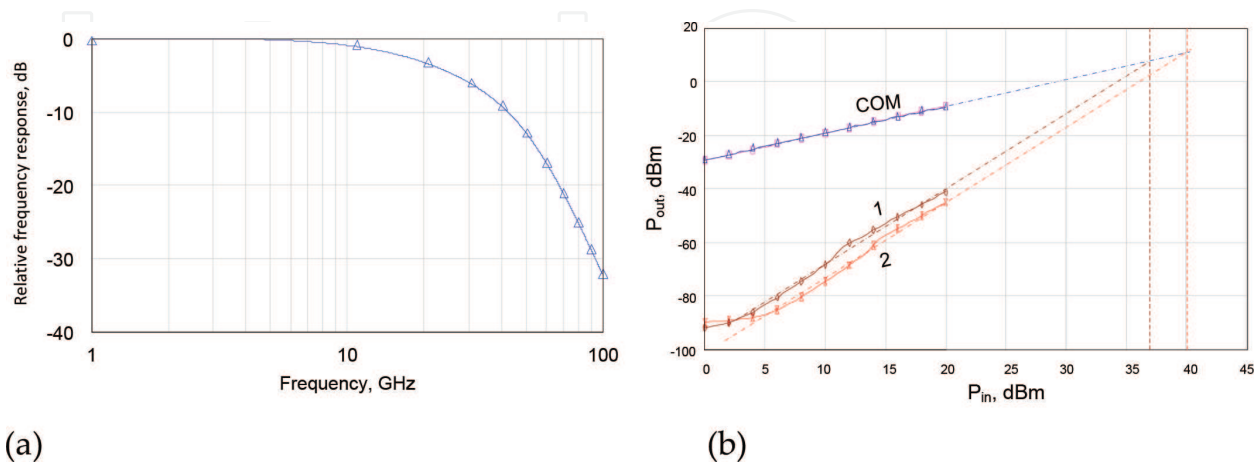**Figure 14.** AWRDE model of a balanced photodetector.

(a)

(b)

Figure 15. The examples of simulation experiments: a—small-signal frequency response; b—large-signal transmission characteristics of the single-ended (1) and balanced (2) photodetectors.

photodetector has near 3-dB advantage in linearity. The both conclusions and the OIP3 values (37–40 dBm) received by the simulation are in close coincidence to modern realistic photodetectors [9, 14].

5. Passive optical components

Low-loss, interference-insensible transmitting is the most attractive feature of an optical fiber for diverse processing in photonic area. As a part of a MWP circuit, it may be defined as a medium connecting RF-to-optical and optical-to-RF converters. In general, in comparison with a coaxial cable, the optical waveguide has three orders of magnitude less attenuation, the bandwidth independent of the RF signal frequency, much better weight and size characteristics, as well as the weaker phase-to-temperature dependence of the transmitted RF signal. Nevertheless, the quality of the transmitted signal may deteriorate due to a number of limiting factors, for example, dispersion, reflection, scattering, nonlinearity, etc. Another important advantage of an optical fiber is that it can be used to design extremely narrow-bandwidth pass-band and notch filters. Below, two new AWRDE behavior models of single mode optical fiber and fiber-based ultra-narrow-bandwidth filter are demonstrated and discussed.

5.1. Single-mode fiber model

Figure 16 depicts AWRDE reciprocal models of single-mode optical fiber feasible for various operating regimes of a realistic fiber-optic link. The first model (**Figure 16(a)**) represents the transmission on a single optical carrier with multiple modulating RF signals (so-called, subcarrier multiplexed mode). Here, a set of limiting factors are taken into account, such as chromatic dispersion, time delay, loss, temperature dependence of characteristics, as well as cross-interference between RF channels.

The basic element for the model of **Figure 16(a)** is the library model of ideal transmission line with loss (TLINP). A mode propagating across the line is specified by its effective dielectric constant and per-unit-length attenuation at user specified frequency. The model scales loss with evaluation frequency. In the model, the frequency band of one 100-GHz optical channel is divided into 16 discrete bands of equal width (more than 6 GHz). Each of them is provided by one TLINP with values of the dielectric constant and attenuation corresponding to a central frequency of a specific band. All TLINPs have the same length, equal to the length of the optical fiber, and are combined using ideal multiplexer models (MUX). The first MUX shares the spectrum of the quasi-optical signal between 16 sections, each of which exploits the corresponding TLINP. The second MUX restores the signal spectrum.

Besides, the second model (**Figure 16(b)**) represents the transmission on a multiple optical carriers (so-called, wavelength division multiplexed (WDM) mode). Here, a cross-interference noise between the carriers is added to the above limiting factors. The main element of each QO channel (CHL) is subcircuit (SUBCKT "CHL"), which structure is discussed above for a single spectral channel. Sixteen SUBCKT "CHL" ones correspond to 16 standard channels of the
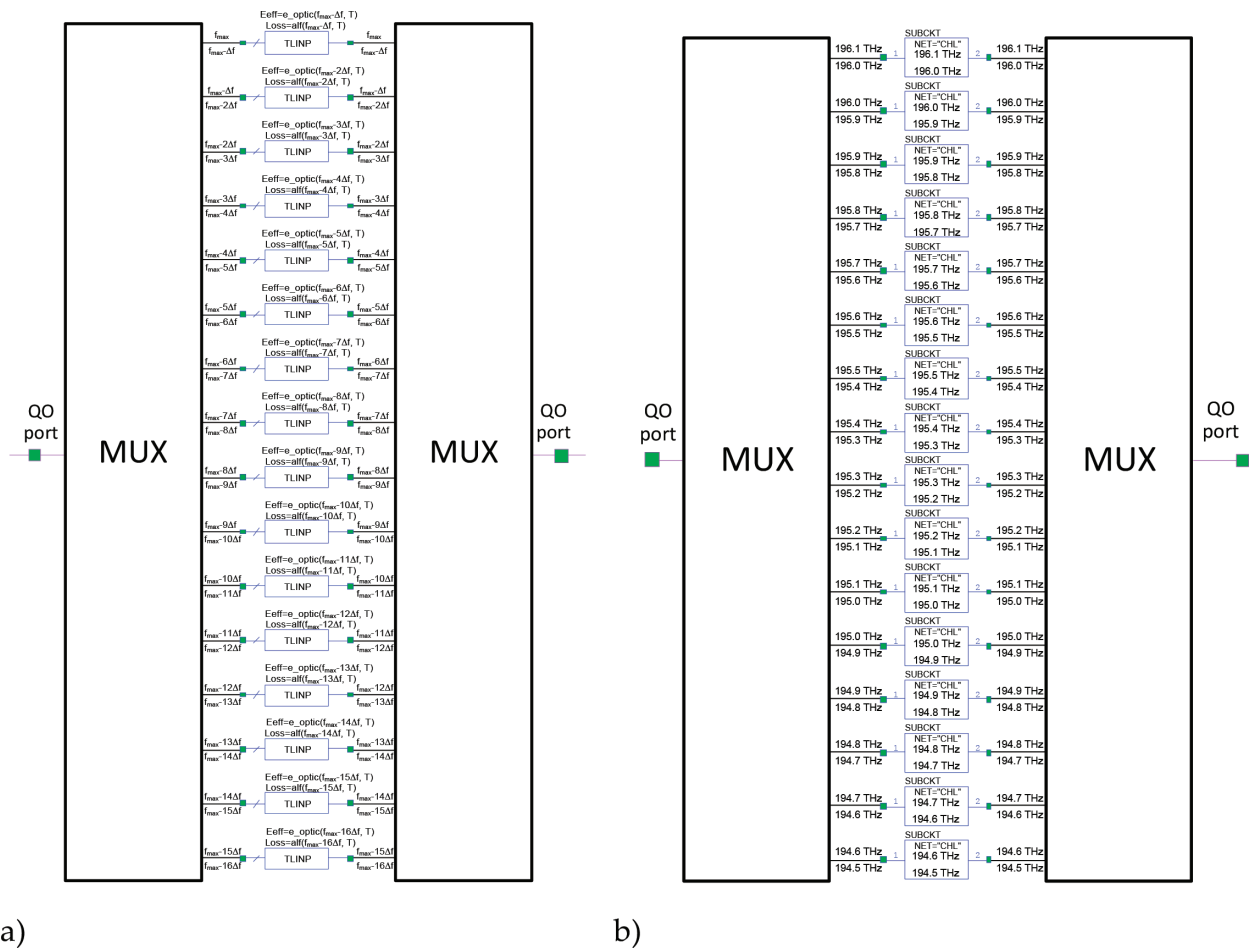
Figure 16. AWRDE models of single-mode optical fiber in various operating regimes: (a) with subcarrier multiplexed mode; and (b) with wavelength division multiplexed mode.

WDM system, so the overall number of RF channels to be transmitted simultaneously is 256. In the model, all SUBCKT "CHL" groups are combined/divided using the same MUX library models that provide the distribution of the input QO spectra according to the corresponding
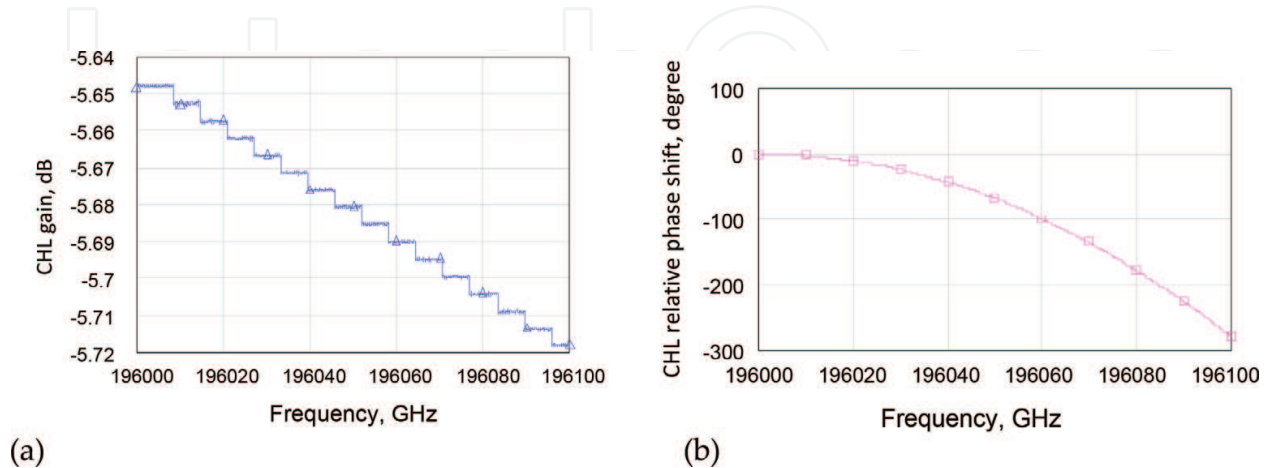

Figure 17. The examples of simulation experiments: (a) QO channel gain versus QO frequency of single-mode optical fiber; (b) QO channel relative phase shift versus QO frequency of single-mode optical fiber.

subcircuits over the single fiber and further restoration of the group spectrum. The schematic can be re-tuned to another bandwidth of QO channels by changing the internal model settings.

Figure 17 exemplifies the simulation results for the both types of single-mode optical fiber models under consideration at room temperature, where QO frequency dependences of CHL gain (a) and of CHL relative phase shift (b) for the fiber length of 30 km are simulated. As seen, the average normalized loss (inverse to gain) is near 0.19 dB/km that equal in this frequency band to the same parameter of standard SMF-28 fiber. In additional, the difference in losses for one 100-GHz optical channel does not exceed 0.07 dB only. Besides, normalized phase-to-temperature shift of RF signal being transmitted over fiber is near 0.1°/GHz/km/°C that corresponds to known data [14].
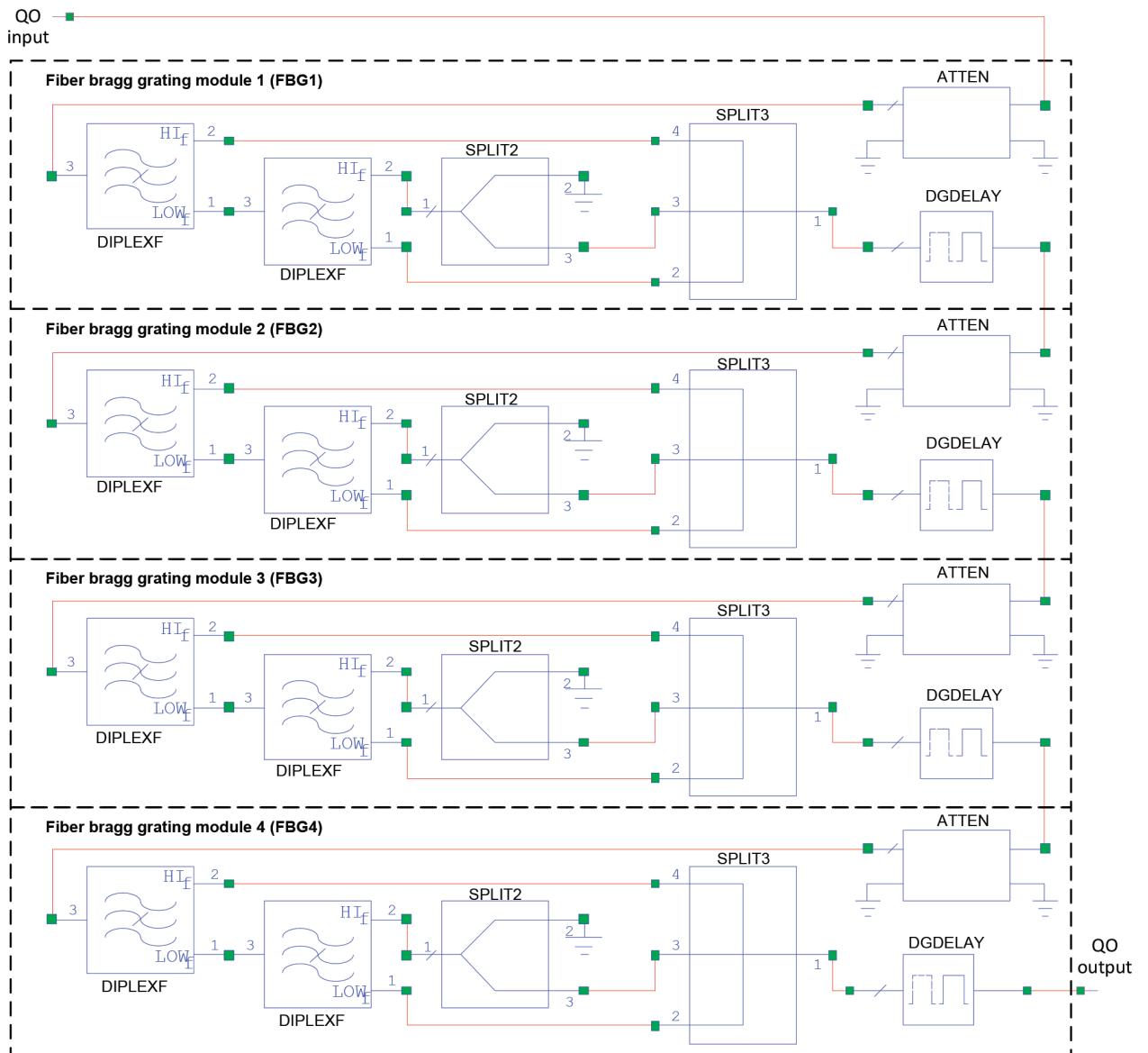
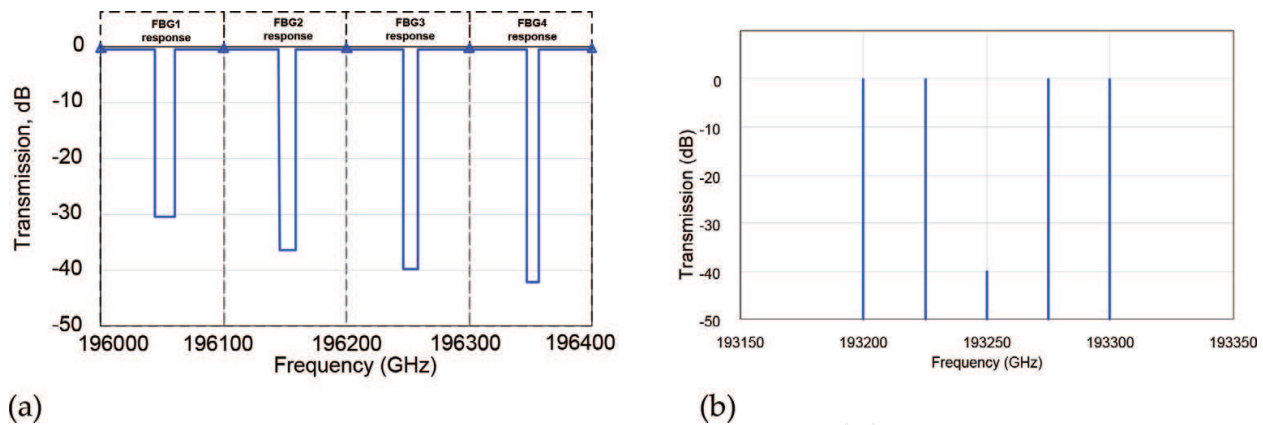**Figure 18.** Four-channel AWRDE notch Bragg grating filter model.

Figure 19. The examples of simulation experiments.

5.2. Narrow-band multichannel optical filter model

Another important element of **Figure 1**'s photonic area used for processing RF signals (filtration, delay) is the notch Bragg grating (NBG), whose optical bandwidth may be as narrow as some hundreds of MHz. **Figure 18** shows 4-channel AWRDE NBG model. Fiber Bragg grating module of each channel (FBG1-FBG4) consists of two library models of ideal passive frequency diplexer DIPLEXF each of them specifies two frequency ranges (low and high) to extract the cutoff band at the output of the second DIPLEXF. In each of the channels, through output 2 of the first DIPLEXF and output 1 of the second DIPLEXF, power is allocated outside the cut-off band. This power is summed by the model SPLIT3 and fed to the next channel. The SPLIT2 unit provides the reflection of the main power in the dedicated band and the transition of some of this power to the next channel (for SPLIT2: S_{21} = 0 dB and S_{31} = −30 dB), thus incomplete reflection is modeled. The residual power from the output 3 of the element SPLIT2 is fed to the element SPLIT3, where it is summed with the signal power outside the cut-off band. The closed-form models of attenuator (ATTEN) and ideal digital time delay element (DGDELAY) insert the attenuation and time delay of the optical signal in each of the Bragg grating channel, respectively.

Figure 19 exemplifies the simulation results for 4-channel NBG filter transmission response (a) and the QO spectrum at the output of the filter model when the same power QO signals inside the band of FBG3 are inputted. As seen, a rejection level of 40 dB is provided.

6. Simulation of microwave-photonics-based RF circuits

In the previous sections, the requisite active and passive AWRDE models for the MWP circuit design were demonstrated and the results of the key simulation experiments were highlighted. Following them, below we will describe some models and modeling results for MWP circuits as the enablers for time-delay processing in photonic area.

6.1. Fiber-optic delay line of RF-signals

Fiber-optic delay line (FODL) is one of the most feasible units of MWP circuitry [14]. The layout of single-channel FODL is very simple and consists of RF/O converter, single-mode optical fiber of a corresponding length (delay ≈ 4.8 ns/m), and O/RF converter. **Figure 20** shows the AWRDE model of single-channel FODL including in order a single-carrier model of semiconductor laser (see Section 2.1, **Figure 2**), a model of single-mode optical fiber (see Section 5.1, **Figure 16(a)**), and a model of PIN photodetector (see Section 4, **Figure 13**) as subcircuits.

Figure 21 exemplifies the simulation results for RF-dependence phase shift and delay of the RF pulse. In particular, **Figure 21(a)** represents the relative phase shift versus frequency of RF signal modulating optical carrier that propagates over the fiber length of 1 m (the delay is near 4.8 ns). As follows from the figure, the phase shift increases linearly with frequency and its slope is approximately 1700° per GHz, which is consistent with the theory of RF delay lines. Besides, **Figure 21(b)** demonstrates the oscillogram of the input and output RF pulses for the fiber length of 3 m. As seen, due to the wide modulation band embedded in the laser and photodetector models (**Figures 3(a)** and **15(a)**, correspondingly), the delay of the radio pulse is exclusively determined by the retarding effect in the optical fiber.

6.2. Temperature-compensated fiber-optic delay line of RF signals

The key issue in realistic FODLs is a fiber thermal instability in operating conditions, because the temperature variations result in remarkable phase shift and the corresponding group time delay changes of the RF signals that is invalid for a set of important applications. There are two
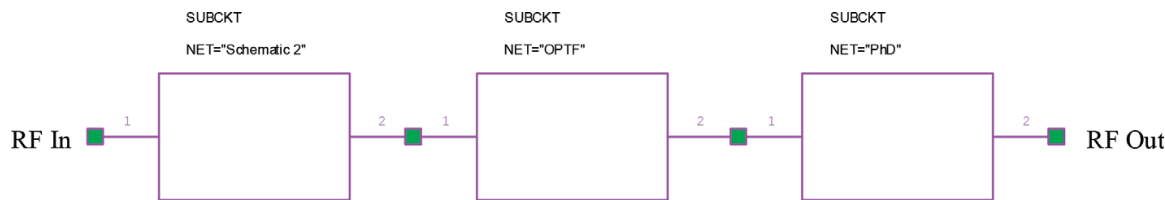
Figure 20. AWRDE model of single-channel fiber-optic delay line of RF signals.
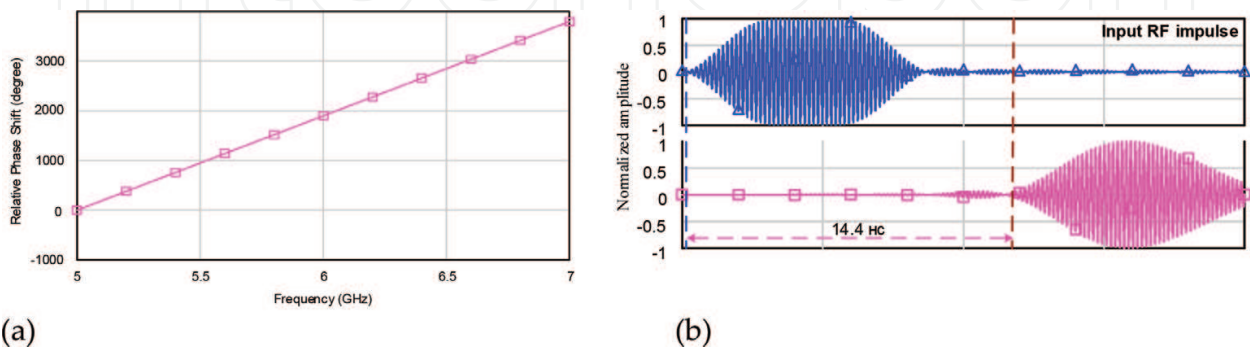
Figure 21. Examples of the simulation results for single-channel FODL of RF signals.

main directions to design temperature-compensating fiber-optic delay lines (TC-FODL) including feedback or phase conjugation concept. The disadvantage of the first one is the limited adjustment range of the RF device, the phase of which is to be regulated depending on the temperature variation. **Figure 22** shows the layout explaining the principle of the second concept that is free of the above shortcoming [18]. In the scheme, the effect of compensation of the temperature-induced change in the delay time is provided by synchronous variation of the fiber length during the triple pass of the modulated by RF frequency optical signal along the same fiber. A detailed explanation of the operation principle for this scheme is given in [18].

Figure 23 demonstrates the proposed ultra-wideband AWRDE model of TC-FODL simulating the operation principle of the schematic in the **Figure 22**. Therein, according to the scheme, the frequency F_m of the input RF signal, first of all, is divided in half and multiplied by one and a half times. The converted frequencies are allocated using library models of bandpass filters BPFB, each of which is tuned to the appropriate frequency. Further, the double trip of the optical carries on the frequencies v_1 and v_2 modulated by the RF signal of frequency $1/2F_m$ is represented by means of the semiconductor laser models (**Figure 4**), the optical fiber model of **Figure 16(b)**, and the photodetector models of **Figure 13**. Finally, in the result of mixing double converted RF signal of frequency $1/2F_m$ with RF signal of frequency $3/2F_m$ using library model MIXER, the input RF signal of frequency F_m is recovered exploiting the library model BPFB
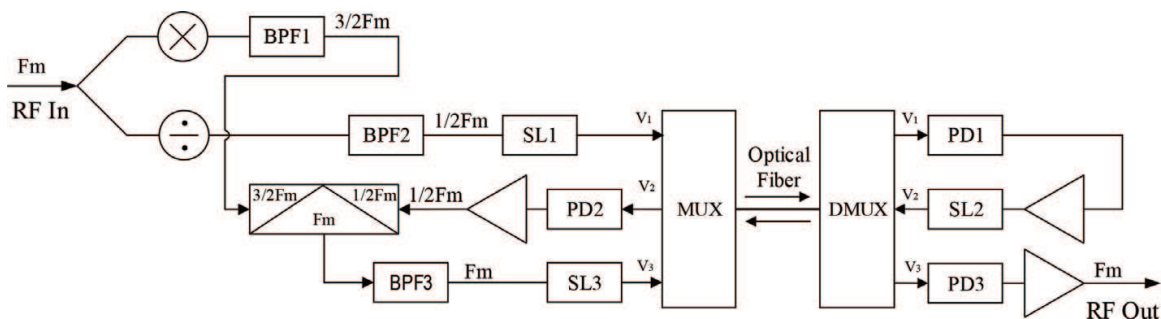

Figure 22. Temperature-compensated fiber-optic delay line of RF signals.
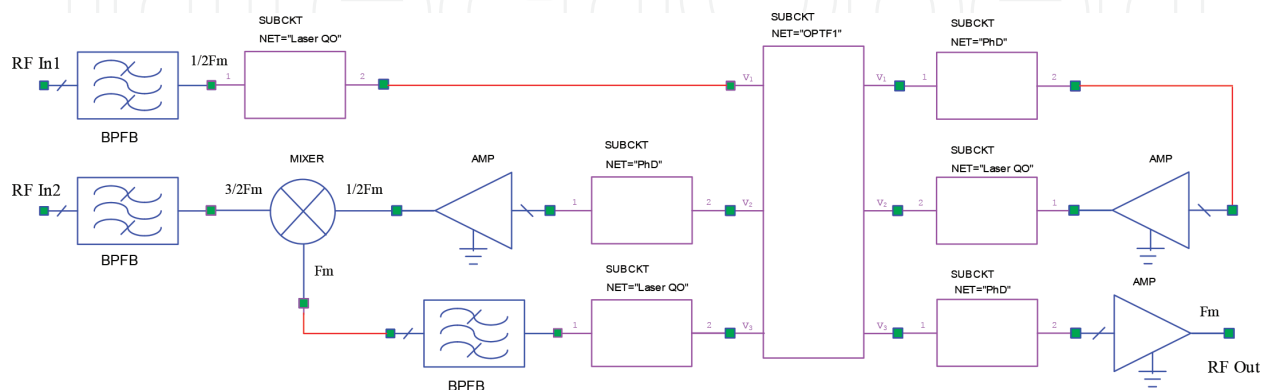

Figure 23. AWRDE model of temperature-compensated fiber-optic delay line of RF signals.
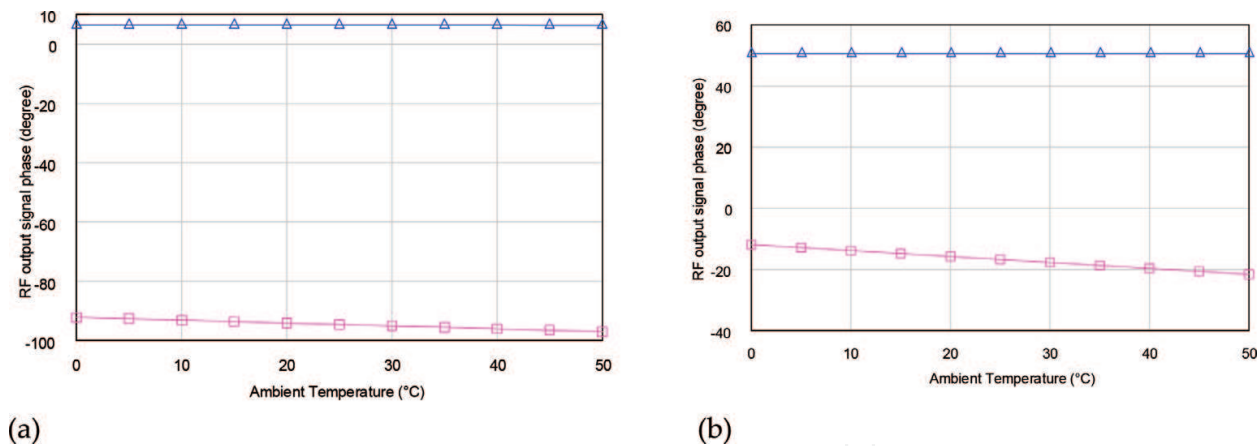
Figure 24. Examples of the simulation results for TC-FODL of RF signals: (a) RF frequency 2.5 GHz; and (b) RF frequency 5 GHz.

and the output after one more trip over TC-FODL on the optical carrier v_3 that are imitated by the separate models of laser and photodetector and the same model of optical fiber.

Figure 24 exemplifies the simulation results for the proposed TC-FODL model of 40 m in length examining its phase-to-temperature characteristics at the RF frequencies of 2.5 GHz (a) and 5 GHz (b) that are performed by triangles. For comparison, the same plots include the simulation results for the FODL model of **Figure 20** that are performed by squares.

Based on the graphs, the following resume can be drawn. Despite the much higher stability of the silica fiber's phase-to-temperature characteristic compared to the coaxial cable [14], the FODL under the study without compensation (the model of **Figure 20**) introduces the phase distortion increasing at higher frequencies of RF signal that is unacceptable in many practical cases. This distortion regardless of RF signal frequency is eliminated by using a special MWP circuit, the example of which was modeled above.

7. Conclusions

In the chapter, a new approach to design the equipment for a future generation of microwave-band radar, electronic warfare, and wireless telecom systems based on microwave photonics technology using well-known microwave-electronic software tool NI AWRDE is proposed and discussed. As a first part of it, updated and new models of key active and passive elements for microwave-photonic circuits were considered that perform direct and external RF-to-optical conversion and processing of RF signals in the optical range, which leads to an improvement in such important characteristics as size, weight and power, electromagnetic and environmental compatibilities, and immunity to external interferences. As an outcome of the conducted simulation experiments, it was shown that the main parameters and characteristics of the optoelectronic and optical elements considered correspond to the real product analogs. In particular, the comparative modeling has verified that the highest level of linearity, superior to modern transistor amplifiers, is provided in the process of external RF-to-optical conversion

by means of an Mach-Zehnder optical modulator and in the process of optical-to-RF conversion using a PIN photodetector. The results of the experimental comparison against the main part of the above-simulated characteristics, which validate the accuracy of the proposed models, are described elsewhere [5–13].

Based on the element models and results of simulations, in the second part of the chapter, we presented two new AWRDE models and the results of model experiments for fiber-optic delay line that realized time-delay processing of RF signals in photonic area. In the course of the model experiment, the way of eliminating phase distortions of delayed RF signal caused by the fluctuation of the ambient temperature under the conditions of application was confirmed.

Acknowledgements

Conflict of interest

The authors declare the lack of the "conflict of interest."

Author details

Mikhail E. Belkin[1]*, Vladislav Golovin[2], Yuri Tyschuk[2], Mikhail G. Vasil'ev[3] and Alexander S. Sigov[1]

*Address all correspondence to: belkin@mirea.ru

1 Moscow State Technological University (MIREA), Scientific and Technological Center "Integrated Microwave Photonics", Moscow, Russian Federation

2 Sevastopol State University (SevSU), Sevastopol, Russian Federation

3 Kurnakov Institute of General and Inorganic Chemistry, Russian Academy of Sciences, Moscow, Russian Federation

References

[1] Izutsu M, Itoh T, Sueta T. 10 GHz bandwidth traveling-wave LiNbO$_3$ optical waveguide modulator. IEEE Journal of Quantum Electronics. June 1978;**14**(6):394-395

[2] Seeds AJ, Williams KJ. Microwave photonics. Journal of Lightwave Technology. 2006;**24**(12):4628-4641

[3] Capmany J, Novak D. Microwave photonics combines two worlds. Nature Photonics. 2007;**1**(1):319-330

[4] Waterhouse R, Novak D. Realizing 5G. IEEE Microwave Magazine. 2015;**16**(8):84-92

[5] Belkin ME, Iakovlev V, Sigov AS, Tyschuk Y, Golovin V. An advanced approach to simulation of super-wide bandwidth information and communication systems combining microwave and photonic industrial technologies. European Modelling & Simulation Symposium (EMSS2016). Cyprus; 26–28 Sept. 2016. pp. 141-147

[6] Belkin ME, Golovin V, Tyschuk Y, Sigov AS. A simulation technique for designing next-generation information and communication systems based on off-the-shelf microwave electronics computer tool. International Journal of Simulation and Process Modeling (IJSPM). 2018. (In print)

[7] Belkin ME, Belkin L, Sigov AS, Iakovlev V, Suruceanu G, Kapon E. Performances of microwave-band analog signal transmission using wafer-fused long wavelength VCSELs. IEEE Photonics Technology Letters. 2011;**23**(20):1463-1465

[8] Belkin ME, Iakovlev V. Microwave-band circuit-level semiconductor laser modeling. In: EMS 2015: 9th European Modeling Symposium on Mathematical Modeling and Computer Simulation. Madrid, Spain; 2015. pp. 1-3

[9] Belkin ME. Multiscale computer aided design of microwave-band P-I-N photodetectors. In: Gateva S, editor. Photodetectors. Croatia: InTech; 2012. pp. 231-250

[10] Belkin ME, Sigov AS. Circuit-level large-signal modeling of microwave bandwidth photodetector. International Conference on Electromagnetics in Advanced Applications ICEAA 2015 Torino; Italy; 7-11 Sept. 2015. pp. 1587-1589

[11] Belkin ME, Golovin V. Microwave electronic CAD modeling of microwave-band optoelectronic oscillator based on long wavelength VCSEL. In: COMCAS 2015: Proceedings of the International Conference on Microwaves, Communications, Antennas and Electronic Systems; Tel Aviv. Israel. pp. 1-3

[12] Belkin ME, Tyschuk Y. Microwave electronic CAD modeling of microwave photonic devices based on LW-VCSEL mixing. In: ICMAP 2015: Proceedings of the II International Conference on Microwave and Photonics; Dhanbad, Bihar. India. pp. 1-3

[13] Belkin ME, Golovin V, Tyschuk Y, Sigov AS. Comparison of RF photonics-based beamformers for super-wide bandwidth phased array antennas. IOP Conference Series: Materials Science and Engineering. 2017;**198**:1-4

[14] Urick VJ, McKinney JD, Williams KJ. Fundamentals of Microwave Photonics. New Jersey: Hoboken; 2015

[15] Fukano H, Akage Y, Kawaguchi Y, Suzaki Y, Kishi K, Yamanaka T, Kondo Y, Yasaka H. Low chirp operation of 40 Gbit/s electroabsorption modulator integrated DFB laser module with low driving voltage. IEEE Journal of Selected Topics in Quantum Electronics. 2007;**13**(5):1129-1134

[16] Yu PKL, Wu MC. Photodiodes for high performance analog links. In: Chang WS, editor. RF Photonic Technology in Optical Fiber Links. University of Cambridge, England: Cambridge university press; 2002. pp. 231-254

[17] Belkin ME, Dzichkovski NA. Research of microwave-bandwidth p-i-n photodetectors. In: EUROCON 2009; St. Petersburg; May 2009. pp. 193-196

[18] Yin F, Zhang A, Dai Y, Ren T, Xu K, Li J, et al. Phase-conjugation-based fast RF phase stabilization for fiber delivery. Optics Express. January 2014;**22**(1):878-884